Ultra-High Loading of Coal-Derived Flash Graphene Additives in Epoxy Composites

Paul A. Advincula, Wei Meng, Lucas J. Eddy, Jacob L. Beckham, Ivan R. Siqueira,*
Duy Xuan Luong, Weiyin Chen, Matteo Pasquali,* Satish Nagarajaiah,*
and James M. Tour*

Graphene has proved to be an exceptional reinforcing additive for composites, but the high cost of its synthesis has largely prevented its addition on industrial scales. Flash Joule heating provides a rapid, bulk-scale method for graphene synthesis from coal materials, such as metallurgical coke (MC), into metallurgical coke-derived flash graphene (MCFG). Here, this work investigates the properties of graphene-epoxy composites in a higher nanofiller content regime than has previously been reported in literature. Composites with 20 to 50 wt% loading of MCFG are prepared by combining MCFG with diglycidyl ether bisphenol A epoxy precursor (DGEBA) and 1,5-diamino-2-methylpentane. With a 1:2 ratio of MCFG:DGEBA, the Young's modulus increases by 92% and with a 1:3 ratio, hardness increases by 140%. At a 1:4 ratio of MCFG:DGEBA, compressive strength and maximum strain increase by 145% and 61%, respectively. At a 1:3 ratio of MCFG:DGEBA, toughness increases by 496%. Finally, at a 1:1 ratio of MCFG:DGEBA, GHG emissions, water consumption, and energy consumption are reduced by 33%, 47%, and 34%, respectively. As the cost of FG plummets, since it can be produced from very low cost materials like MC, in milliseconds with no solvent or water, the prospects are promising for its high-loading use in composites.

1. Introduction

Epoxy resins are a commonly used class of thermosetting polymeric materials with a wide variety of applications, such as coatings, adhesives, and composites. This is due to their ease of processability, high mechanical strength, chemical and corrosion resistance, and thermal stability.[1] Epoxies exhibit a high degree of crosslinking, which give them high rigidity and strength. However, this same phenomenon makes them brittle and vulnerable to cracks.[2] Diglycidyl ether bisphenol A (DGEBA) is one of the most popular epoxy resins due to its outstanding chemical and mechanical properties, including processability at low temperatures and good wettability to reinforcing additives.[3,4] The properties of such materials can often be enhanced through addition of carbon nanomaterials[5,6] since these nanomaterials possess outstanding mechanical,

P. A. Advincula, L. J. Eddy, J. L. Beckham, D. X. Luong, W. Chen,
M. Pasquali, J. M. Tour
Department of Chemistry
Rice University
6100 Main Street, Houston, TX 77005, USA
E-mail: mp@rice.edu; tour@rice.edu
W. Meng, S. Nagarajaiah
Department of Civil and Environmental Engineering
Rice University
6100 Main Street, Houston, TX 77005, USA
E-mail: satish.nagarajaiah@rice.edu

L. J. Eddy
Applied Physics Program
Rice University
6100 Main Street, Houston, TX 77005, USA
I. R. Siqueira, M. Pasquali
Department of Chemical and Biomolecular Engineering
Rice University
6100 Main Street, Houston, TX 77005, USA
E-mail: ir16@rice.edu
D. X. Luong, M. Pasquali, S. Nagarajaiah, J. M. Tour
Smally-Curl Institute for Nanoscale Science and Technology
Rice University
6100 Main Street, Houston, TX 77005, USA
M. Pasquali, S. Nagarajaiah, J. M. Tour
Department of Materials Science and NanoEngineering
Rice University
6100 Main Street, Houston, TX 77005, USA
M. Pasquali
The Carbon Hub
Rice University
6100 Main Street, Houston, TX 77005, USA

thermal, and electrical properties.[7] This can improve the toughness of the epoxies, making them less brittle. Carbon fibers have been used in previous reports to obtain high filler content in epoxy composites. However, the high cost of carbon fibers has slowed their widespread use.[8] Other methods for obtaining high loadings of nanofillers include use of buckypapers[9] and aerogels,[10] which are limited by their high cost and difficulty of production.

One such nanomaterial, graphene, has been shown to be an effective reinforcing additive for epoxies. Consisting of a honeycomb sheet of carbon atoms, graphene was disclosed in 2004 by Novoselov and Geim through micromechanical graphite cleavage using adhesive tape.[11] The unique structure of graphene imparts it with outstanding thermal, electrical, and mechanical properties.[12–14] However, the high cost of producing graphene using traditional energy- or chemical-intensive processes has prevented its use on an industrial scale.[15] Techniques such as mechanical and chemical exfoliation,[11] chemical oxidation or reduction,[16,17] shear exfoliation,[18] and others[19] produce graphene that costs between $60 000 to $200 000 per ton, depending on the quality of the product.[20,21] No technique has yet been able to provide ton-scale bulk-scale production of high-quality graphene.

Additionally, the loading of the filler is often limited by several factors. Higher loadings lead to increased viscosity of the pre-curing mixture, resulting in a decrease in mechanical strength of the final composite due to insufficient dispersion of the filler in the composite. The decrease in mechanical properties can also be attributed to the lack of interfacial interactions between the matrix and filler.[22] Without further functionalization, such as treatment with O_3/H_2O, van der Waals forces tend to dominate the interface between graphene and the surrounding polymer matrix.[23] This native interface creates weak points in the mechanical transfer of stress from the matrix to the nanofiller. As such, for most graphene-type materials, the optimal range of loading is as low as 0.1 to 0.5 wt%, with some reports reaching as high as 8 wt%.[2,24–32] The high aspect ratio of graphene (between 500 and 2000)[33] means that mechanical property enhancements can be obtained at relatively small loadings, which is advantageous due to the high cost of conventionally produced graphene.[34] Addition of graphene materials has been shown to enhance mechanical properties,[35,36] EMI shielding,[37] and electrical properties[38,39] of epoxy composites.

Recently, our group demonstrated that flash Joule heating (FJH) could be used to synthesize flash graphene (FG) from a variety of different feedstocks, including plastic waste,[20] coffee grounds,[40] rubber tires,[41] and carbon black.[42,43] The resulting FG is turbostratic[44] and more thermally stable than comparable reduced graphene oxide materials produced from conventional

techniques, such as the Hummer's method.[45] These properties make FG ideal for use as an additive to composites.

Different grades of coal have been found to be ready feedstocks for conversion into graphene using flash Joule heating. Annual consumption of coal is estimated to fall from 5.25 billion tons in 2020 to 600 million tons by 2050, due to the growth of renewable energy sources, such as solar and wind power.[46] Hence, the coal industry and coal-producing locales are continually searching for alternative applications of coal materials. Composition and properties of carbon sources vary according to type, such as anthracitic coal, charcoal, calcined coke, and petroleum coke. Each of these examples have been successfully converted into FG.[40] Additionally, metallurgical coke (MC) has been found to be one of the best feedstocks for FJH, due to its high carbon content, conductivity, and purity.[47,48]

==The aim of this study is to incorporate metallurgical coke-derived flash graphene (MCFG) into DGEBA epoxy at high loading ratios, ranging from 20–50%, and prepare a graphene-epoxy composite with improved mechanical properties.== Until recently, such high loadings of graphene were impractical due to the cost and availability of graphene, but FG has changed that metric. While other nanomaterials have also been shown to be effective additives to epoxies, MCFG is used due to the low cost of materials and conversion relative to current alternatives, which enables its use on an industrial scale, as well as its efficacy as a reinforcing additive. The optimum loading of MCFG, where the ratio of mechanical property enhancement to loading is maximized, likely occurs at lower loadings, but here we explore the use of MCFG as both a reinforcing and filling additive to reduce the cost and environmental impacts of the matrix material, hence the high loading ratios. Conventionally produced graphene is limited to low wt% loadings due to its high cost, whereas MCFG could later become free of such restrictions.
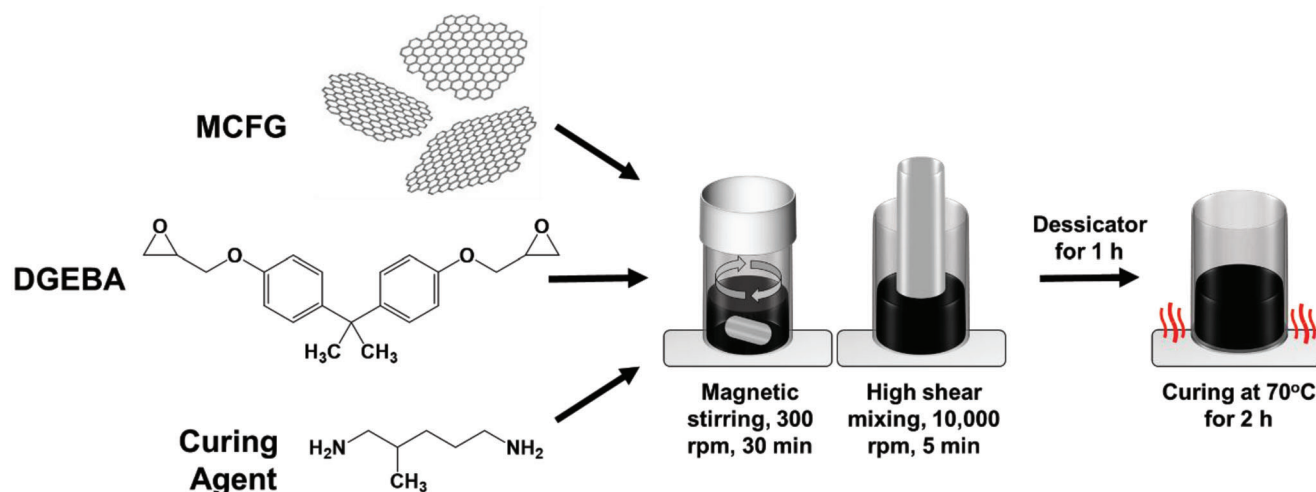
MCFG is prepared by FJH of MC using a flash Joule heater. This MCFG is then mechanically stirred, and shear mixed with DGEBA epoxy and 1,5-diamino-2-methylpentane curing agent in a single vial. After curing, micro- and macro-scale mechanical testing of the composites shows significant improvement in the materials' Young's modulus, hardness, maximum strain, compressive strength, and toughness. Due to the low cost of producing MCFG through FJH, MCFG can act as both a reinforcing additive and as a filler material to strengthen and replace epoxy in a composite material, as well as provide an alternative, environmentally friendly application of coal materials as determined here by a preliminary life cycle analysis.

2. Results and Discussion

DGEBA, MCFG, and curing agent (1,5-diamino-2-methylpentane) are combined in a 20 mL scintillation vial, as shown in **Figure 1**. A magnetic stir bar is then used to stir the solution. To enhance the shearing and dispersion of the MCFG in the resin, high shear mixing is then applied to the solution. Finally, the epoxy resin is cured and crosslinked by heating the solution at 70 °C for 2 h without a cap. This process ensures that the MCFG is well-dispersed throughout the epoxy resin, without use of solvents.

To ensure that the graphene used in this composite material was good quality, the MCFG was characterized using Raman

S. Nagarajaiah
Department of Mechanical Engineering
Rice University
6100 Main Street, Houston, TX 77005, USA

J. M. Tour
Welch Institute for Advanced Materials
Rice University
6100 Main Street, Houston, Texas 77005, USA

**ADVANCED
SCIENCE NEWS**

www.advancedsciencenews.com

**[M]acromolecular
Materials and Engineering**

www.mame-journal.de

**Figure 1.** Schematic illustration of the preparation of MCFG:DGEBA composites.

spectroscopy and X-ray diffraction (XRD). Analysis of graphene usually depends on three prominent active phonon modes. These include the 2D ($\approx$2700 cm^{-1}), G ($\approx$1580 cm^{-1}), and D bands ($\approx$1350 cm^{-1}). The 2D mode appears because of an overtone of the in-plane transverse optic branch (iTO). The G band usually appears in graphitic carbon as a response to an in-plane phonon mode. The D peak is seen when there are graphene edges or structural defects present in the sample. The ratio of I_{2D}/I_G peaks is indicative of the quality and number of layers of graphene in AB-stacked graphene. The FJH process produces turbostratic graphene, meaning that the interlayer spacing between sheets increases and the sheets of graphene are rotated about the axis normal to the sheets.[41] As such, the intensity of the 2D peak increases as the number of graphene layers increases. Normally, in the case of AB-stacked graphene, more layers result in loss of desirable 2D material properties as interlayer electron transport increases. Turbostratic graphene retains its 2D properties, even with more layers, because interlayer electron transport is reduced by the increased interlayer spacing. Examining the I_D/I_G ratio also yields useful information about the degree of disorder in the sample, where a higher ratio is indicative of a greater amount of disorder.

Figure 2a,c compares the average Raman spectra and mapping data of the MC feedstock and MCFG. FJH of the MC into MCFG results in a rise in average I_{2D}/I_G ratio from 0.109 to 0.596. Additionally, the I_D/I_G ratio is reduced from 0.835 to 0.551. Together, these indicate that the amorphous carbon of MC is converted into MCFG. FG yield is calculated by finding the percentage of spectra that meet the following criteria: 1) minimum I_{2D}/I_G ratio of $\geq$0.3, 2) signal-to-noise ratio of >5 in the 2D band region, and 3) 2D band with a FWHM of <100 cm^{-1}. Prior to FJH, none of the MC spectra qualify as graphene, but after FJH, 95.9% of the spectra qualify as graphene, indicating the high conversion of MC into MCFG. Process yield, calculated as the mass after FJH divided by the mass prior to FJH, is also high for MC, being $\approx$95%. This is consistent with the high carbon content of MC (Figures S2–S4, Supporting Information). The resulting flakes are also quite large, being up to $\approx$0.75 µm on average in size (Figure S5, Supporting Information).

XRD is also useful for verifying the type of stacking in the graphene sheets. Typical AB-stacked graphene, such as in graphite nanoplatelets, often have a narrow (002) peak at 26.4°.[41] Turbostratic graphene has increased interlayer spacing as a result of the rotation of graphene layers. As such, MCFG (Figure 2b) has a (002) peak that shifts to a lower diffraction angle (26.1°) and increases in FWHM.[51] The much larger FWHM of MC indicates that MC is amorphous. The increased intensity and narrower (002) peak of MCFG relative to MC indicates that the MCFG is converted to graphene. The low intensity of 3D peaks, such as the (101) and (102), which appear at 45° and 50°, respectively, are also indicative that MCFG lacks three-dimensionality. Raman spectroscopy and XRD definitively show the conversion of MC into high-quality, turbostratic MCFG, respectively.

Composites of MCFG and liquid epoxy resin (DGEBA) were blended with a 1,5-diamino-2-methylpentane curing agent in a single 20 mL scintillation vial. After stirring, high shear mixing, and curing, the vial was cut with a diamond saw blade and broken to extract the composite material before sanding (**Figure 3**a,b). Raman spectroscopy was used to determine whether the MCFG is well dispersed throughout the epoxy matrix. Each sample of MCFG:DGEBA showed that >85% of spectra could be identified as graphene (Figure 3c), indicating the good dispersion of MCFG in the epoxy.

Thermogravimetric analysis (TGA) is used to confirm the uptake of MCFG in DGEBA (Figure 3d). Degradation of the epoxy appears to occur in two main stages. Between 350 and 450 °C, $\approx$75% of the epoxy degrades, corresponding presumably to unreacted curing agent, dehydration of hydroxyl groups, and pyrolysis of crosslinked epoxy resin. Between 450 and 600 °C, degradation of the remaining 25% is likely the decomposition of cyclized or aromatic byproducts.[52] When MCFG is added to the epoxy system, a third stage is introduced, corresponding to the degradation of MCFG, beginning between 528 to 567 °C, with this temperature increasing as the proportion of MCFG increases. Degradation of the epoxy follows the same trend as before, with $\approx$75% of the epoxy degrading between 350 to 450 °C and the remaining $\approx$25% degrading between 450 °C and the onset degradation
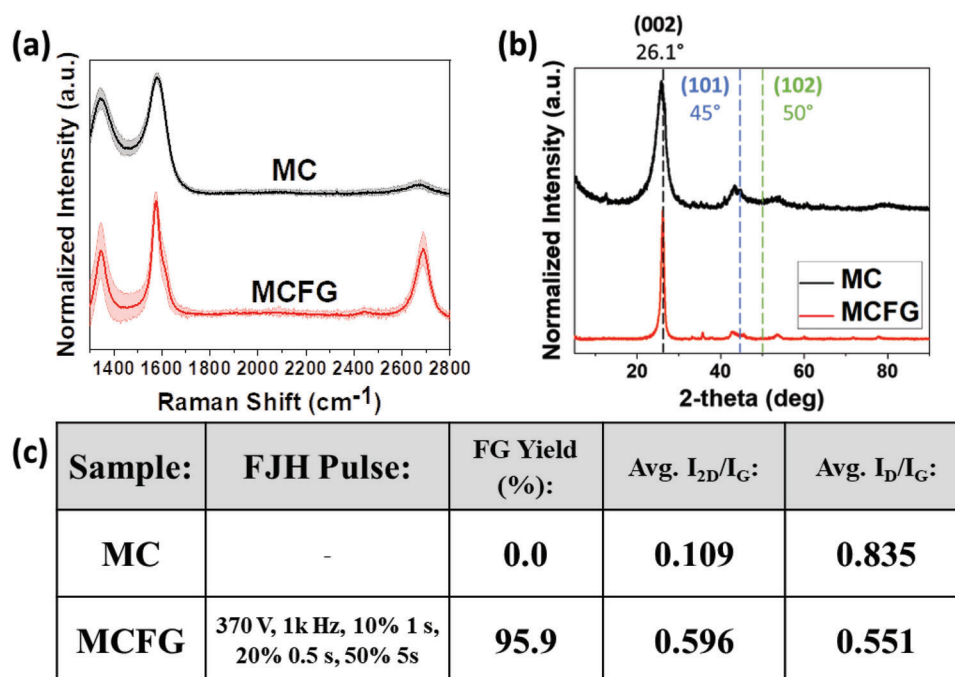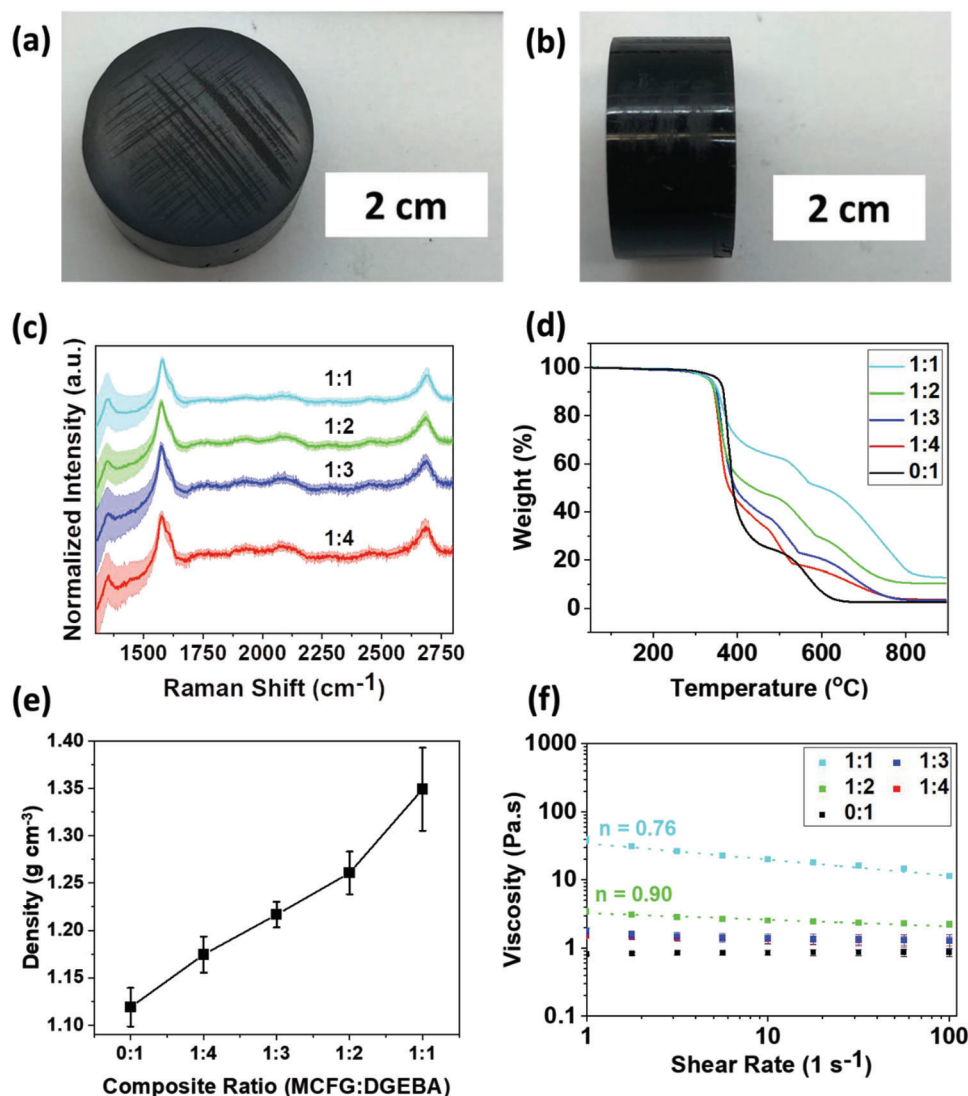
Figure 2. Characterization of the MC and MCFG. a) Average Raman spectra with standard deviation shown by shaded regions ($N = 100$), b) XRD spectra with dashed lines indicating the positions of the (002), (101), and (102) peaks, and c) yield and intensity ratios of the MC and MCFG, as determined by Raman spectroscopic analysis.

Sample:	FJH Pulse:	FG Yield (%):	Avg. I_{2D}/I_G:	Avg. I_D/I_G:
MC	-	0.0	0.109	0.835
MCFG	370 V, 1k Hz, 10% 1 s, 20% 0.5 s, 50% 5s	95.9	0.596	0.551

temperature of the MCFG in that sample. This decrease in degradation temperature for the cyclized or aromatic byproducts is likely due to decreased crosslinking because of the presence of MCFG nanofillers. At a 1:1 ratio of MCFG:DGEBA, 50% of the total mass remains at the onset of MCFG degradation. At a 1:2 ratio, ≈33% of the mass remains. These are consistent with the initial loadings of MCFG in the epoxy. This trend continues in the 1:3 and 1:4 ratios of MCFG:DGEBA.

The densities of three samples at each ratio were calculated (Figure 3e). Compared to the neat epoxy, the density of 1:4 MCFG:DGEBA is 0.06 g cm^{-3} higher. The density continues to increase as the loading of MCFG increases, with a maximum density increase of 0.23 g cm^{-3} for the 1:1 MCFG:DGEBA composite. Finally, the viscosity of each sample was analyzed as a function of shear rate ($N = 2$), as seen in Figure 3f. Moderate increases in viscosity are observed as the ratio of MCFG:DGEBA is increased from 0:1 to 1:2. However, the viscosity of these slurries is still low enough to be stirred with a magnetic stir bar, even with a 1:2 ratio of MCFG:DGEBA. Viscosity increases with particle loading, which is to be expected for general particulate systems.[53] This increase is still substantially small compared to carbon nanotube solutions, likely because MCFG has a lower aspect ratio of ≈482 (see Section 4).[54] At a ratio of 1:1 MCFG:DGEBA, the viscosity significantly increases, resulting in decreasing workability of the slurry. Fitting the data with the power-law model, the power-law index (n) is found to be 0.90 and 0.76 for the 1:2 and 1:1 ratios, respectively, indicating weak shear-thinning behavior. "Average" viscosities of each slurry can be found in Table S1, Supporting Information, where the average of all measurements across the range of tested shear rates is calculated.

Triboindentation was used to characterize the microscale mechanical properties of the MCFG:DGEBA composites. When compared to neat epoxy, the surface of 1:1 MCFG:DGEBA has clearly visible areas which are graphene-rich (**Figure 4**a,b). These flakes can potentially be responsible for variation in the measurements, an effect described by Han et al.[7] Each sample of MCFG:DGEBA, including the neat epoxy, was indented to a contact depth of 1000 nm. The maximum load for neat epoxy was ≈2.7 mN. This load increased as the loading of MCFG increased, to a maximum of ≈6.1 mN for the 1:2 composite (Figure 4c). Further increases in MCFG loading to a ratio of 1:1 led to a decrease in maximum load to 4.5 mN. This could be due to decreasing crosslinking density in the composite because of rising viscosity from increasing MCFG loading. The average triboindentation curves indicate that at the same contact depth, the composites with MCFG required more force to achieve the same depth than the neat epoxy. Analysis of these results demonstrates that addition of MCFG to the epoxy matrix results in significant increases to the mechanical properties of the resin (Figure 4d). The maximum increase in hardness of 140% is obtained at a 1:3 ratio of MCFG:DGEBA. A 92% increase in Young's modulus is observed at a 1:2 ratio of MCFG:DGEBA. At a 1:1 ratio of MCFG:DGEBA, both Young's modulus and hardness begin to decrease, likely due to the increased viscosity of the 1:1 ratio slurry which leads to reduced crosslinking of the epoxy and aggregation of MCFG.

Compressive testing demonstrates that the addition of MCFG to the epoxy resin results in improved mechanical properties. Similar or improved Young's moduli are observed for each composite material, as well as significantly increased maximum compressive strengths and strains to failure. The roughness in the region after the linear portion of the stress–strain curves for higher

ADVANCED
SCIENCE NEWS
www.advancedsciencenews.com

[M]acro-molecular
**Materials and Engineering**
www.mame-journal.de

Figure 3. Optical images of a) top and b) side view of a typical MCFG:DGEBA composite. c) Average Raman spectra with standard deviation shown by shaded regions ($N = 100$) and d) TGA profiles of MCFG:DGEBA composites. The temperature was ramped from 50 to 900 °C with a heating rate of 15 °C min^{-1}. All samples were run under an atmosphere of air. e) Density measurements of MCFG:DGEBA composites ($N = 3$). f) Viscosity flow curve of MCFG:DGEBA composites ($N = 2$). The shear thinning index, n, for the 1:2 and 1:1 MCFG:DGEBA slurries is indicated. Ratios denote the proportion of MCFG to DGEBA.

ratio composites is likely due to the formation of pores and holes within the epoxy, because of the increased viscosity of the higher ratio composites before curing (**Figure 5**a).

Compressive strength is increased by 145% and the maximum strain is increased by 61% in the 1:4 ratio of MCFG:DGEBA (Figure 5b). Toughness of the composites is optimized in the 1:3 ratio of MCFG:DGEBA, with an increase of 496%. Further addition of MCFG decreases the toughness, with the 1:1 ratio being almost the same as the neat epoxy. Addition of MCFG particularly affects the toughness, maximum stress, and strain in tensile testing, where significant decreases are observed (Figure S6, Supporting Information). This is likely due to the increasing in solution viscosity which arises as FG proportion is increased, leading to entrapment of air bubbles and voids, which can be observed

under scanning electron microscopy (SEM) (Figure S7, Supporting Information).

Finally, the environmental impact of nanofiller addition to a matrix should be considered. Use of a reinforcing additive to strengthen a composite means that less material is required for a given application, thereby reducing cost and environmental impact. Filler additives can achieve the same effect if production of the filler is less expensive and less resource-intensive to produce. MCFG has shown potential to fulfill both roles. In addition to enhancement of mechanical properties, replacing DGEBA with MCFG results in a significant decrease in GHG emissions, water consumption, and energy consumption (**Figure 6**). At a 1:1 ratio, GHG emissions are reduced by 33%, water consumption is reduced by 47%, and energy consumption is reduced by 34%.
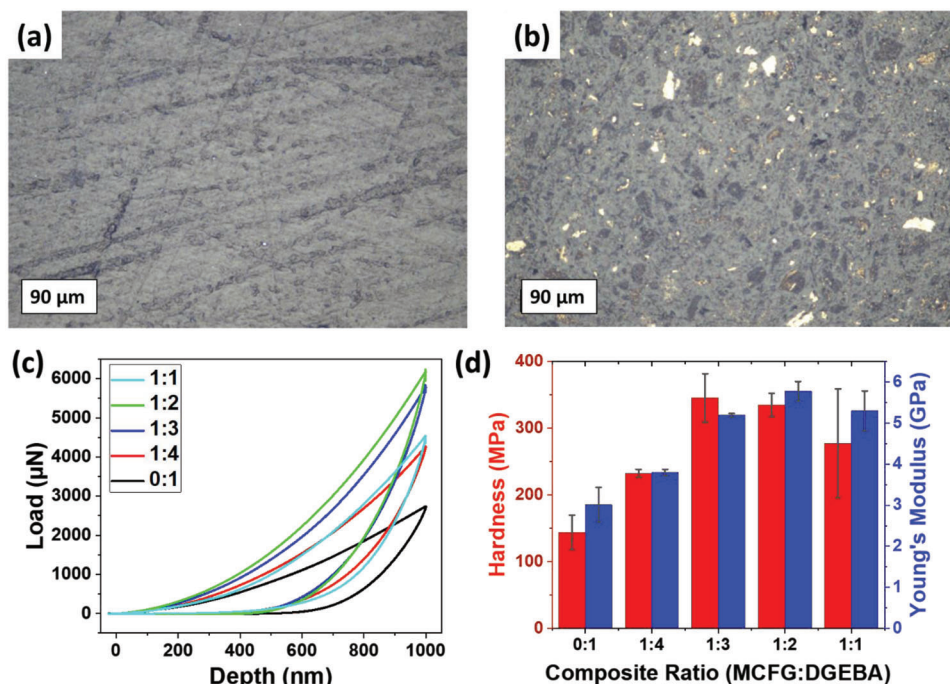
Figure 4. Characterization of microscale mechanical properties. Optical microscope images of the surfaces of a) 0:1 and b) 1:1 MCFG:DGEBA composites. c) Representative force–displacement curves using a Berkovich indenter tip with a pyramidal geometry and d) indentation modulus and hardness measurements of MCFG:DGEBA composites ($N = 5$). Ratios denote the proportion of MCFG:DGEBA.
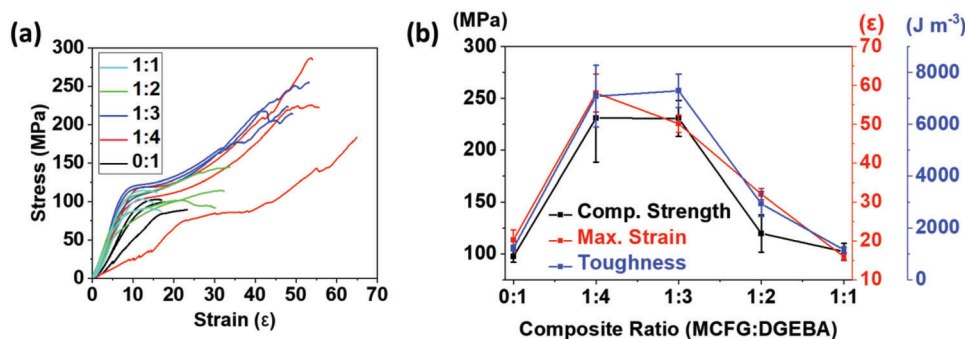
Figure 5. Characterization of macroscale mechanical properties. a) Compressive stress–strain curves and b) mechanical property measurements for MCFG:DGEBA composites ($N = 3$). Toughness measurements were evaluated by calculating the area under the stress–strain curve of each samples. Ratios denote the proportion of MCFG:DGEBA.

At the best performing ratio of 1:3, GHG emissions, water consumption, and energy consumption are reduced by 17%, 23%, and 17%, respectively. Improvements in the FJH process, such as increased batch size and decreased energy density might further reduce GHG commissions, water consumption, and energy consumption.

Process input and output data for epoxy production, metallurgical coke production, and electricity usage for the FJH process were based on literature.[55] Transportation of material and waste stream disposal/remediation were defined as being outside the scope of this study. Background data was sourced primar-

ily from Argonne National Laboratory's GREET model including GREET.Net software and spreadsheet models. References, sources, and detailed tables of the processes are shown in Tables S2 and S3, Supporting Information.

3. Conclusions

Composites made from MCFG and DGEBA epoxy resin have been successfully prepared through a simple, one-pot process involving shear mixing and mechanical stirring. The high MCFG uptake of the matrix material enables replacement of between
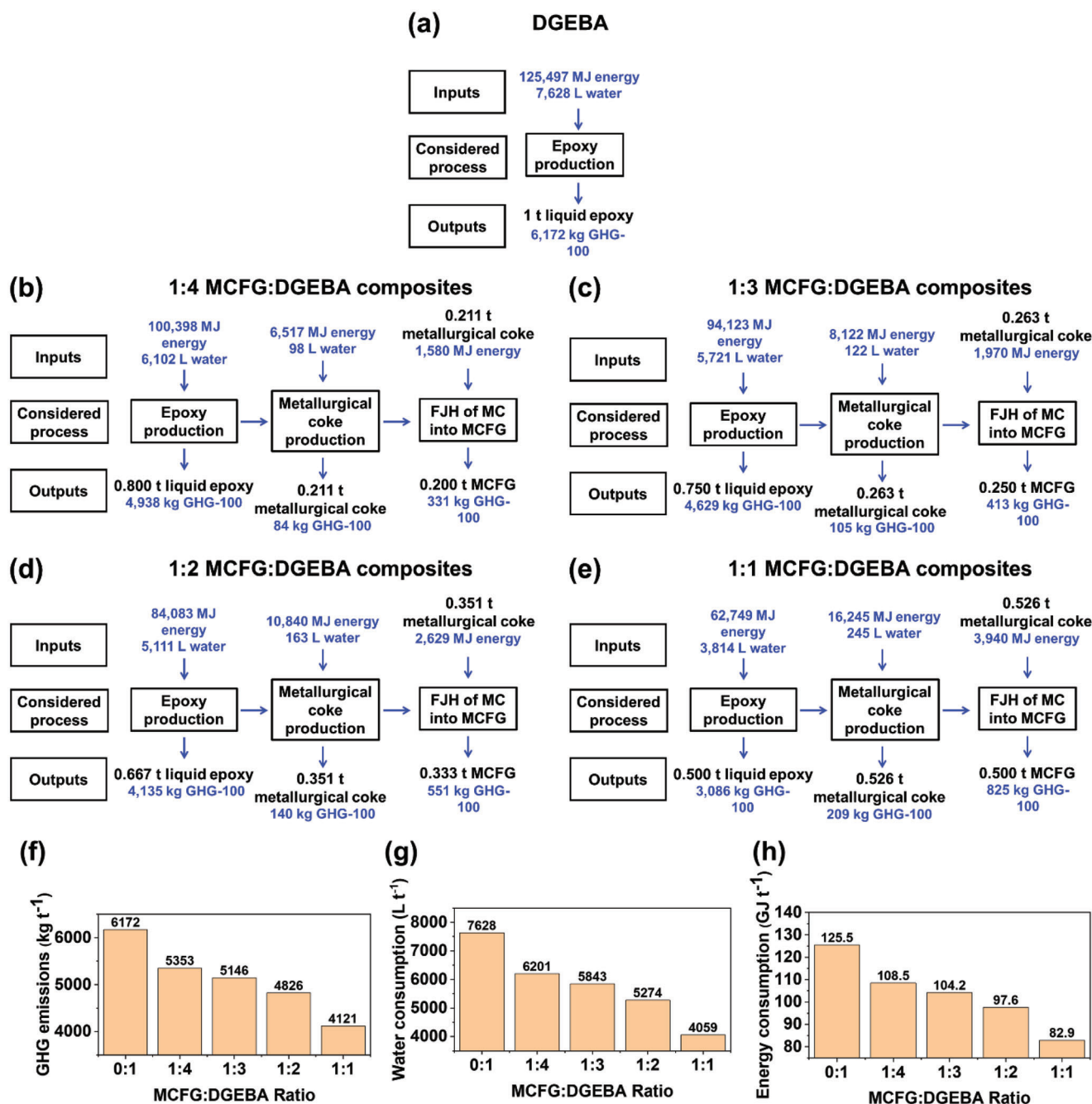
Figure 6. Flow chart of production of equivalent masses of a) neat epoxy, b) 1:4, c) 1:3, d) 1:2, and e) 1:1 MCFG:DGEBA composites. Comparison of f) GHG emissions, g) water consumption, and h) energy consumption for neat epoxy and MCFG:DGEBA composites.

20 to 50% of the epoxy resin with high-quality, turbostratic graphene. Addition of MCFG as a reinforcing additive increases the mechanical properties of the material. Young's modulus, hardness, maximum compressive strength, and maximum strain can be increased by 92%, 140%, 145%, and 61%, respectively, under optimized conditions. Toughness can also be improved by 496%. The low cost of MCFG production through FJH also enables it to act as a filler replacement for the epoxy resin, with only an increase in density between 0.06 to 0.23 g cm^{-3}.

This technology could result in increased usage of FG as both a reinforcing additive and a filler in epoxy composite applications, reducing costs and emissions because of the material's improved performance and because of MCFG's lower energy consumption, water consumption, and GHG emissions, compared to neat epoxy. This technique also provides an environmentally friendly alternative application for coal and coal-derived materials as their annual consumption is predicted to fall.

4. Experimental Section

Materials: MC was obtained from SunCoke Energy and ground into various sizes. MCFG was prepared by sieving ground MC with a #12 and #20 sieve. The portion of MC that was smaller than #12 and larger than #20, corresponding to particles 1.68–0.841 mm in diameter, was then subjected to a variable FJH pulse with duty cycles of 10%, 20%, and 50%, for 1, 0.5, and 5 s, respectively. A pulse of 370 V and 1000 Hz frequency was used to produce MCFG. The MCFG was then ball-milled with steel balls at a weight ratio of 100:15 steel balls:MCFG for 2 h at 400 rpm. DGEBA was obtained from Millipore-Sigma (Lot #: MKCK4566) and used as received. 1,5-diamino-2-methylpentane was obtained from Millipore-Sigma (Lot #: SHBG9920V) and used as received.

Composite Preparation: MCFG:DGEBA composites were prepared by combining 6.0 g of DGEBA with 0.9 g of 1,5-diamino-2-methylpentane in a 20 mL scintillation vial. The solution was mixed with a magnetic stir bar for 30 min at 300 rpm. During this mixing, 0.0 to 6.0 g of MCFG was slowly poured into the vial, depending on the desired loading ratio of MCFG. After stirring, the solution was then shear mixed with homogenizer obtained from Cole–Parmer (Tissue Tearor 986370–07 Homogenizer; 120 VAC, 1.2A) for 5 min at ≈10 000 rpm. The solution was then placed in a vacuum desiccator for 1 h to remove any remaining air bubbles. Once degassed, the composite was cured on a hot plate for 2 h at ≈70 °C, then allowed to cure at room temperature overnight. After curing was complete, the scintillation vial was broken and the remaining composite was ground with an abrasive wheel, then with 100, 800, 1000, 1200, and 2500 grit sandpaper to remove the remaining glass and shape the composite to the appropriate dimensions for mechanical testing.

Raman Spectroscopy: Raman spectra were collected with a Renishaw inVia confocal Raman microscope using a 532 nm laser. A 50× objective lens was used with a laser power of 5 mW to scan the samples from 1300 to 2800 cm^{-1}. Large-area Raman mapping was used to determine the crystallinity and morphology of the graphene by analysis of the spectra with a custom-written Python script using the RamPy package. Collected spectra were background-corrected, and a Savitsky–Golay filter was used to smooth the spectra before quantification of graphene yield and peak ratios. To qualify as graphene, three criteria were used to assess individual spectra: 1) a minimum I_{2D}/I_G ratio of ≥0.3, 2) a signal-to-noise ratio of >5 in the 2D band region, and 3) a 2D band with a full width at half-maximum (FWHM) of <100 cm^{-1}.

XRD: XRD data of ball-milled MCFG was collected and analyzed on a Rigaku SmartLab II instrument with zero background sample holders. Collection was carried out with a scan width of 0.02° step^{-1} and a scan rate of 2° min^{-1}. The X-ray wavelength was 0.154 nm. Thickness of FG was calculated using the Scherrer equation (Equation (1)):[49]

$$t = \frac{0.89\lambda}{\beta \cos\theta} \tag{1}$$

Here, t is the out of plane crystallite thickness, λ is the x-ray wavelength, β is the FWHM of the (002) peak in radians, and θ is the diffraction angle of the (002) peak. Aspect ratio is calculated by dividing the lateral flake size (obtained through transmission electron microscopy; TEM) by the thickness of the flakes.

X-Ray Photoelectron Spectroscopy: X-Ray Photoelectron Spectroscopy (XPS) data of ball-milled MCFG were collected using a PHI Quantera SXM Scanning X-ray microprobe maintained at 5×10^{-9} Torr. Survey spectra were recorded with a step size of 0.5 eV at a pass energy of 140 eV. Elemental spectra were collected using a 0.1 eV step size at a pass energy of 26 eV. Peak fitting was carried out using a Shirley baseline collection.

TGA: TGA was carried out using alumina pans in a Mettler Toledo TGA/DSC 3+ system. The temperature was ramped from 50 to 900 °C with a heating rate of 15 °C min^{-1}. All samples were run under an atmosphere of air.

Triboindentation: Nanoindentation was carried out using a Hysitron TI 980 Triboindenter equipped with a Berkovich tip with a pyramidal geometry. To calculate the indentation modulus and hardness, at least five different indentations were performed for each sample with a maximum displacement of 1000 nm and a displacement rate of 10 nm s^{-1}. Elastic modulus and hardness were calculated using the Oliver Pharr approach, employing Equations (2)–(4).[7,50]

$$E_r = \frac{\sqrt{\pi}}{2}\frac{S}{\sqrt{A_P}} \tag{2}$$

$$\frac{1}{E_r} = \frac{1-\nu^2}{E} + \frac{1-\nu_i^2}{E_i} \tag{3}$$

$$H = \frac{P}{A_P} \tag{4}$$

where E_r is the reduced elastic modulus; S is the stiffness of the initial part of the unloading curve; A_P is the projected area of contact; E and ν are the elastic modulus and Poisson's ratio of the sample, respectively; E_i and ν_i are the elastic modulus and Poisson's ratio of the indenter, respectively; H is the hardness; and finally, P is the applied load.

Compressive Testing: Stress–strain curves were obtained through uniaxial compressive tests at room temperature with a standard compressive testing machine (MTS Model 312.21). Samples of varying thickness (10 to 16 mm) and similar diameter (≈25 mm) were held between two crossheads, checked to avoid misalignment, and then compressed at a constant rate of 2 mm min^{-1}. Three samples of each ratio of MCFG:DGEBA were tested to ensure consistency of the results. Strain was calculated based on the individual thickness of each sample, given the varying thicknesses.

Tensile Testing: Tensile stress–strain curves were obtained by testing samples on a uniaxial tension machine (MTS 858 Material Testing System) with a 0.4 mm min^{-1} loading rate. Load and displacement were recorded by loading cell and linear variable differential transformer, respectively. Three samples of each ratio of MCFG:DGEBA were tested to ensure consistency of the results. Stress was calculated by dividing the force by the cross-section of each sample. Dimensions of the tensile samples are shown in Figure S1, Supporting Information. The thickness of each sample was ≈0.18 cm.

TEM: Dilute solutions (≈1 mg mL^{-1}) of MCFG in ethanol were sonicated (Cole–Parmer 750 watt ultrasonic processor with a cup horn) for 15 min prior to drop-casting onto a 200 mesh Cu grid with lacey carbon film. A JEOL 2100F field-emission gun TEM at 200 kV was used to image the sample.

SEM: The fracture surfaces of the tensile samples were attached to SEM stubs using double-sided carbon tape and imaged using a FEI Helios NanoLab 660 DualBeam SEM system at 500 V with a current of 0.1 μA.

Viscosity Measurements: Viscosity was measured with an Ares G2 Rheometer (TA Instruments) using a parallel plate fixture (25 mm diameter, 0.9 mm gap). Samples were tested immediately after mixing. Shear rate was varied between 1 to 100 s^{-1} (a range over which the measured torque was safely within the transducer resolution) and no hysteresis was observed. Slurries with loading ratios of 1:1 and 1:2 MCFG:DGEBA were fitted using the power-law model shown in Equation (5).

$$\eta = K\dot{\gamma}^{n-1} \tag{5}$$

Here, η is viscosity, K the consistency index, $\dot{\gamma}$ the shear rate, and n is the power-law index. If $n = 1$, the material is Newtonian. If $n < 1$, the material is shear-thinning, with stronger shear-thinning behavior observed at smaller values of n.

Supporting Information

Supporting Information is available from the Wiley Online Library or from the author.

Conflict of Interest

The authors declare the following competing financial interest(s): Rice University owns intellectual property on the synthesis and use of FG. That intellectual property has been licensed to a company in which J.M.T. is a stockholder, but not an officer, director, or employee. Conflicts of interest are mitigated through regular disclosure to and compliance with the Rice University Office of Sponsored Programs and Research Compliance. The authors declare no other potential comflicts.

Data Availability Statement

The data that support the findings of this study are available from the corresponding author upon reasonable request.

[1] P. Head, *Eng. Des.* **1996**, *22*, 4.

[2] N. I. C. Berhanuddin, I. Zaman, S. A. M. Rozlan, M. A. A. Karim, B. Manshoor, A. Khalid, S. W. Chan, Q. Meng, *J. Phys.: Conf. Ser.* **2017**, *914*, 012036.

[3] A. Maiorana, S. Spinella, R. A. Gross, *Biomacromolecules* **2015**, *16*, 1021.

[4] R. Auvergne, S. Caillol, G. David, B. Boutevin, J.-P. Pascault, *Chem. Rev.* **2014**, *114*, 1082.

[5] J. Ma, Q. Meng, A. Michelmore, N. Kawashima, Z. Izzuddin, C. Bengtsson, H.-C. Kuan, *J. Mater. Chem. A* **2013**, *1*, 4255.

[6] U. Kilic, M. M. Sherif, O. E. Ozbulut, *Polym. Test.* **2019**, *76*, 181.

[7] X. Han, T. Wang, P. S. Owuor, S. H. Hwang, C. Wang, J. Sha, L. Shen, J. Yoon, W. Wang, R. V. Salvatierra, P. M. Ajayan, R. Shahsavari, J. Lou, Y. Zhao, J. M. Tour, *ACS Nano* **2018**, *12*, 11219.

[8] S. Nunna, P. Blanchard, D. Buckmaster, S. Davis, M. Naebe, *Heliyon* **2019**, *5*, e02698.

[9] Q. Xia, Z. Zhang, Y. Liu, J. Leng, *Composites, Part B* **2020**, *199*, 108231.

[10] G. Gorgolis, C. Galiotis, *2D Mater.* **2017**, *4*, 032001.

[11] K. S. Novoselov, A. K. Geim, S. V. Morozov, D. Jiang, Y. Zhang, S. V. Dubonos, I. V. Grigorieva, A. A. Firsov, *Science* **2004**, *306*, 666.

[12] C. N. R. Rao, A. K. Sood, K. S. Subrahmanyam, A. Govindaraj, *Angew. Chem., Int. Ed.* **2009**, *48*, 7752.

[13] Z. Yan, Z. Peng, Z. Sun, J. Yao, Y. Zhu, Z. Liu, P. M. Ajayan, J. M. Tour, *ACS Nano* **2011**, *5*, 8187.

[14] G. Zhao, T. Wen, C. Chen, X. Wang, *RSC Adv.* **2012**, *2*, 9286.

[15] X.-Y. Wang, A. Narita, K. Müllen, *Nat. Rev. Chem.* **2018**, *2*, 0100.

[16] S. Y. Toh, K. S. Loh, S. K. Kamarudin, W. R. W. Daud, *Chem. Eng. J.* **2014**, *251*, 422.

[17] J. Chen, B. Yao, C. Li, G. Shi, *Carbon* **2013**, *64*, 225.

[18] Y. Hernandez, V. Nicolosi, M. Lotya, F. M. Blighe, Z. Sun, S. De, I. T. Mcgovern, B. Holland, M. Byrne, Y. K. Gun'ko, J. J. Boland, P. Niraj, G. Duesberg, S. Krishnamurthy, R. Goodhue, J. Hutchison, V. Scardaci, A. C. Ferrari, J. N. Coleman, *Nat. Nanotechnol.* **2008**, *3*, 563.

[19] W. Kong, H. Kum, S.-H. Bae, J. Shim, H. Kim, L. Kong, Y. Meng, K. Wang, C. Kim, J. Kim, *Nat. Nanotechnol.* **2019**, *14*, 927.

[20] W. A. Algozeeb, P. E. Savas, D. X. Luong, W. Chen, C. Kittrell, M. Bhat, R. Shahsavari, J. M. Tour, *ACS Nano* **2020**, *14*, 15595.

[21] N. H. Barbhuiya, A. Kumar, A. Singh, M. K. Chandel, C. J. Arnusch, J. M. Tour, S. P. Singh, *ACS Nano* **2021**, *15*, 15461.

[22] D. G. Papageorgiou, I. A. Kinloch, R. J. Young, *Prog. Mater. Sci.* **2017**, *90*, 75.

[23] G. Wang, Z. Dai, L. Liu, H. Hu, Q. Dai, Z. Zhang, *ACS Appl. Mater. Interfaces* **2016**, *8*, 22554.

[24] G. Y. Romero-Zúñiga, D. Navarro-Rodríguez, M. E. Treviño-Martínez, *J. Appl. Polym. Sci.* **2022**, *139*, 51467.

[25] L. Cao, X. Liu, H. Na, Y. Wu, W. Zheng, J. Zhu, *J. Mater. Chem. A* **2013**, *1*, 5081.

[26] S. Khammassi, M. Tarfaoui, Y. Qureshi, H. Benyahia, *Mech. Mater.* **2021**, *158*, 103873.

[27] A. Kesavulu, A. Mohanty, *Polym. Compos.* **2022**, *43*, 2711.

[28] S. Riaz, S.-J. Park, *Materials* **2019**, *12*, 1354.

[29] Z. Barani, F. Kargar, K. Godziszewski, A. Rehman, Y. Yashchyshyn, S. Rumyantsev, G. Cywiński, W. Knap, A. A. Balandin, *ACS Appl. Mater. Interfaces* **2020**, *12*, 28635.

[30] Ö. U. Colak, N. Bahlouli, D. Uzunsoy, C. Francart, *Polym. Test.* **2020**, *81*, 106219.

[31] Z. Liu, Y. Chen, Y. Li, W. Dai, Q. Yan, F. E. Alam, S. Du, Z. Wang, K. Nishimura, N. Jiang, C.-T. Lin, J. Yu, *Nanoscale* **2019**, *11*, 17600.

[32] J. Wei, R. Atif, T. Vo, F. Inam, *J. Nanomater.* **2015**, *2015*, 561742.

[33] S. Morimune-Moriya, T. Goto, T. Nishino, *Nanocomposites* **2019**, *5*, 84.

[34] Y. T. Park, Y. Qian, C. Chan, T. Suh, M. G. Nejhad, C. W. Macosko, A. Stein, *Adv. Funct. Mater.* **2015**, *25*, 575.

[35] A. K. Pathak, M. Borah, A. Gupta, T. Yokozeki, S. R. Dhakate, *Compos. Sci. Technol.* **2016**, *135*, 28.

[36] M. K. Hossain, M. M. R. Chowdhury, N. W. Bolden, *J. Mater. Sci. Eng. A* **2016**, *6*, 117.

[37] Z. Anwar, A. Kausar, L. A. Khan, B. Muhammad, *Nanocomposites* **2016**, *2*, 141.

[38] T. T. Tung, R. Karunagaran, D. N. H. Tran, B. Gao, S. Nag-Chowdhury, I. Pillin, M. Castro, J.-F. Feller, D. Losic, *J. Mater. Chem. C* **2016**, *4*, 3422.

[39] L.-C. Tang, Y.-J. Wan, D. Yan, Y.-B. Pei, L. Zhao, Y.-B. Li, L.-B. Wu, J.-X. Jiang, G.-Q. Lai, *Carbon* **2013**, *60*, 16.

[40] D. X. Luong, K. V. Bets, W. A. Algozeeb, M. G. Stanford, C. Kittrell, W. Chen, R. V. Salvatierra, M. Ren, E. A. Mchugh, P. A. Advincula, Z. Wang, M. Bhatt, H. Guo, V. Mancevski, R. Shahsavari, B. I. Yakobson, J. M. Tour, *Nature* **2020**, *577*, 647.

[41] P. A. Advincula, D. X. Luong, W. Chen, S. Raghuraman, R. Shahsavari, J. M. Tour, *Carbon* **2021**, *178*, 649.

[42] W. Chen, J. T. Li, Z. Wang, W. A. Algozeeb, D. X. Luong, C. Kittrell, E. A. Mchugh, P. A. Advincula, K. M. Wyss, J. L. Beckham, M. G. Stanford, B. Jiang, J. M. Tour, *ACS Nano* **2021**, *15*, 11158.

[43] W. Chen, C. Ge, J. T. Li, J. L. Beckham, Z. Yuan, K. M. Wyss, P. A. Advincula, L. Eddy, C. Kittrell, J. Chen, D. X. Luong, R. A. Carter, J. M. Tour, *ACS Nano* **2022**, *16*, 6646.

[44] M. G. Stanford, K. V. Bets, D. X. Luong, P. A. Advincula, W. Chen, J. T. Li, Z. Wang, E. A. Mchugh, W. A. Algozeeb, B. I. Yakobson, J. M. Tour, *ACS Nano* **2020**, *14*, 13691.

[45] P. A. Advincula, A. C. De Leon, B. J. Rodier, J. Kwon, R. C. Advincula, E. B. Pentzer, *J. Mater. Chem. A* **2018**, *6*, 2461.

[46] IEA, *Int. Energy Agency* **2021**, 224, https://www.eia.gov/coal/production/quarterly/pdf/t17p01p1.pdf (accessed: 14 Dec 2022).

[47] K. M. Wyss, R. D. De Kleine, R. L. Couvreur, A. Kiziltas, D. F. Mielewski, J. M. Tour, *Comms. Eng.* **2022**, *1*, 3.

[48] J. L. Beckham, K. M. Wyss, Y. Xie, E. A. Mchugh, J. T. Li, P. A. Advincula, W. Chen, J. Lin, J. M. Tour, *Adv. Mater.* **2022**, *34*, 2106506.

[49] Y. Gao, O. T. Picot, E. Bilotti, T. Peijs, *Eur. Polym. J.* **2017**, *86*, 117.

[50] W. C. Oliver, G. M. Pharr, *J. Mater. Res.* **1992**, *7*, 1564.

[51] Z. Q. Li, C. J. Lu, Z. P. Xia, Y. Zhou, Z. Luo, *Carbon* **2007**, *45*, 1686.

[52] R. Wang, T. P. Schuman, *eXPRESS Polym. Lett.* **2012**, *7*, 272.

[53] R. G. Larson, *The Structure and Rheology of Complex Fluids*, Oxford University Press, Oxford **1999**.

[54] V. A. Davis, L. M. Ericson, A. N. G. Parra-Vasquez, H. Fan, Y. Wang, V. Prieto, J. A. Longoria, S. Ramesh, R. K. Saini, C. Kittrell, W. E. Billups, W. W. Adams, R. H. Hauge, R. E. Smalley, M. Pasquali, *Macromolecules* **2004**, *37*, 154.

[55] G. Keoleian, S. Miller, R. De Kleine, A. Fang, J. Mosley, *Life Cycle Material Data Update for GREET Model*, University of Michigan, Ann Arbor, MI **2012**, p. 214.